

NUMERICAL SIMULATION OF THE HIGH-FREQUENCY OSCILLATORY VENTILATION IN GENERIC MODELS OF THE HUMAN AIRWAYS

Daniel Feldmann

Institute of Aerodynamics and Flow Technology
German Aerospace Center (DLR)
Göttingen, Germany
daniel.feldmann@dlr.de

Claus Wagner

Institute of Aerodynamics and Flow Technology
German Aerospace Center (DLR)
Göttingen, Germany
claus.wagner@dlr.de

ABSTRACT

To improve the understanding of the gas transport mechanisms under conditions of high-frequency oscillatory ventilation (HFOV) we perform numerical simulations of the unsteady flow in simplified models of the human airways using time varying Dirichlet boundary conditions (BC) for the pressure. The flow fields in a generic trachea show excellent agreement with the analytical solution with an average absolute deviation of less than 10^{-2} for non-dimensional frequencies up to $Wo = 14$. Nonetheless, the computational effort increases for high Wo simulations due to a long relaxation phase and strong velocity gradients near the wall despite of relatively low Reynolds numbers. We also simulated the flow within an endo-tracheal tube comprising turbulent as well as laminar flow behaviour throughout the oscillation cycle. Finally, we used the Dirichlet pressure BCs on multiple open outlets at symmetric bifurcation and three-generation airway models, while guaranteeing mass conservation. Employing identical and slightly different pressure values at the distal bifurcation ends, flow fields are reproduced, similar to that occurring under conditions of uneven physiological behaviour of different lung regions (e.g. pendelluft).

INTRODUCTION

High-frequency oscillatory ventilation (HFOV) is an artificial respiration technique employing relatively high "breathing" frequencies up to 15 Hz and very low tidal volumes, usually below the anatomical dead space. It is stated to reduce ventilator associated lung injury (VALI) from overdistension of lung epithelium due to high tidal volumes (volutrauma), excessive alveolar pressure values (barotrauma) as well as cyclic alveolar re-collapse (atelektrauma) and resulting inflammatory response (biotrauma). Therefore, HFOV has great potential to improve clinical results from severe respiratory diseases such as acute respiratory distress syndrome (ARDS) as

stressed by e.g. Krishnan & Brower (2000). However, advancing HFOV from being a rescue means to being an accepted alternative ventilation strategy certainly requires a detailed knowledge of the governing gas transport mechanisms, which highly differ from those in spontaneous breathing. To gain more insight regarding the gas transport, the efforts on experimental investigations have considerably increased in recent years (e.g. Adler & Brücker (2007) and Scholz *et al.* (2010)). The high complexity of pulmonary air flow due to very small and irregular geometries with poor or even without optical access makes numerical investigations essential to supplement such experiments. A lot of numerical studies were conducted on pulmonary airflow under various conditions but only a few considering high frequencies. The most recent and most comprehensive ones were done by Choi *et al.* (2010) and Wall *et al.* (2010), both using time varying Dirichlet boundary conditions (BC) for the velocity with a prescribed profile. Under conditions of HFOV the flow field in the conducting airway region is governed by repeating flow reversals and co-axial counter flows, typical for high Womersley number flows. Additionally, the irregular and multi-bifurcating geometry makes the flow and its impact on gas transport even more complex. Since the velocity distribution in the bronchi under conditions of HFOV is a priori unknown, we use Dirichlet BCs for the pressure at all open boundaries and do not predefine a certain velocity profile, in contrast to the aforementioned studies. Thus, we assume Dirichlet pressure BCs to be more realistic, which further allow for the setting of non-harmonic pressure waves. This is more similar to the flow driving mechanism of common HFOV devices, which are usually pressure-cycle machines. In the present work we discuss the analytical solution for oscillatory pipe flow and the relevant parameter range under conditions of HFOV in the human respiratory system. We also use a pure Dirichlet pressure BCs set-up to simulate oscillatory flow in a pipe, a bifurcation and a three-generation airway geometry.

THEORETICAL BACKGROUND

To describe the flow in the conducting airways we use the continuity equation and the unsteady, incompressible Navier–Stokes equation

$$\partial_j u_j = 0 \quad (1)$$

$$\partial_t u_i + u_j \partial_j u_i = -\frac{1}{\rho} \partial_i p + \nu \partial_j (\partial_j u_i + \partial_i u_j), \quad (2)$$

where u is the velocity and the indices $i, j = 1, 2, 3$ refer to the space coordinates x_i and x_j , respectively. Throughout this paper the working fluid is air which is normally inhaled at ambient temperature and then heated up to body temperature. Hence, we use a density of $\rho = 1.15 \text{ kg/m}^3$ and a kinematic viscosity of $\nu = 1.63 \times 10^{-5} \text{ m}^2/\text{s}$ corresponding to air at an average temperature of 30°C and an ambient pressure of $p = 1000 \text{ hPa}$. Examining oscillatory fluid motions such as respiratory flow, the governing non-dimensional parameters are the Reynolds number and the Womersley number (e.g. Womersley (1955) or Trukenmüller (2006)), defined as

$$Re = \frac{\hat{u} \cdot D}{\nu} \quad \text{and} \quad Wo = \frac{D}{2} \sqrt{\frac{\omega}{\nu}}. \quad (3)$$

Let D be a characteristic bronchi diameter and $\omega = 2\pi f$ the ventilation frequency ranging from $f = 0.2 \text{ Hz}$ for normal breathing up to $f = 15 \text{ Hz}$ for HFVO based ventilation. As a characteristic velocity within one oscillatory cycle T we use the peak velocity $\hat{u} = \max_{0 < t \leq T} \bar{u}(t)$, where

$$\bar{u}(t) = \frac{1}{A} \int_A \vec{u}(\vec{x}, t) d\vec{A} \quad (4)$$

is the instantaneous area-averaged mean velocity.

ANALYTICAL OSCILLATORY PIPE FLOW

For a generic single bronchus, i.e. in our case a simple pipe geometry as sketched in figure 1, we assume a laminar and axially symmetric flow which is also considered to be fully developed. By this we model a low Re flow far away from the inlets as well as periodic in T . Despite the fact that all bronchial tubes are too short and branch up too rapidly to maintain a fully developed flow at all, this straight pipe approximation is suitable as a validation case for our oscillatory

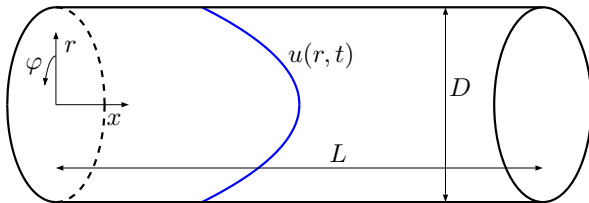


Figure 1. Schematic of a generic bronchus with unsteady velocity profile (blue) of the oscillatory ventilation driven by a sinusoidal varying finite pressure gradient along the x -axis.

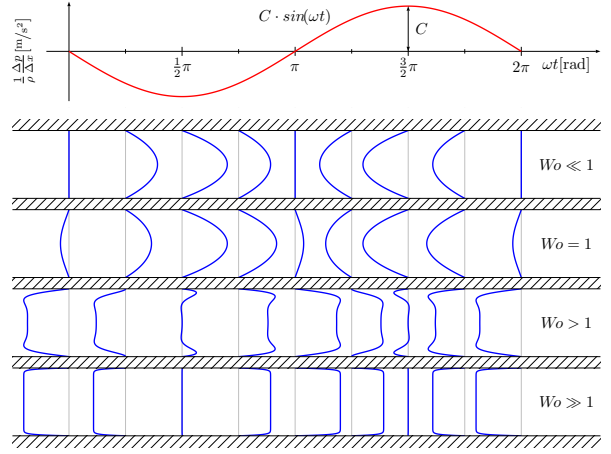


Figure 2. Normalised velocities (blue) in a generic bronchus at eight different points per cycle with respect to the oscillating pressure gradient (red) as obtained from the analytical solution (6) according to Womersley (1955).

flow simulations employing the time varying Dirichlet pressure BC.

In both, spontaneous breathing and most HFOV, the oscillatory flow is driven by a time varying pressure gradient

$$\frac{-1}{\rho} \frac{\partial p}{\partial x} = f(t) \quad \Rightarrow \quad \frac{p_{x=L} - p_{x=0}(t)}{-\rho \cdot L} = C \cdot \sin(\omega t) \quad (5)$$

which we presume to be oscillating in a sinusoidal manner. The restriction to harmonic wave forms is a common simplification for experimental and numerical investigations which holds for spontaneous breathing, whereas most HFOV devices rather apply non-harmonic pressure waves. Using a complex ansatz of the pressure oscillation (5) and the assumptions from above with the momentum equation (2), one finally obtains

$$u(r, t) = -\frac{C}{\omega} e^{i\omega t} \left[1 - \frac{J_0\left(r\sqrt{\frac{i\omega}{\nu}}\right)}{J_0\left(\frac{D}{2}\sqrt{\frac{i\omega}{\nu}}\right)} \right] \quad (6)$$

for the velocity. This equation was derived for the first time by Womersley (1955) and from then on often used in the context of pulmonary and vascular flows. Here, i denotes the imaginary unit and J_0 the Bessel function of first kind and zeroth order. Since the velocity solution is complex, of course, only the real part of equation (6) is of physical relevance. Figure 2 shows radial velocity profiles for the full range of non-dimensional frequencies (3). It is obvious that the oscillatory character of the flow field strongly depends on the Womersley number. For $Wo \ll 1$ the flow appears to be quasi-steady, which means the fluid is able to instantly follow the driving force and the velocity profiles therefore develop a parabolic Hagen–Poiseuille shape at any time. With increasing Wo this shape disappears more and more. The profile deforms and stronger velocity gradients develop close to the wall. Furthermore, positive and negative axial velocity components occasionally co-exist, when flow reversal takes place from inspiration to expiration and vice versa. This is also referred to as

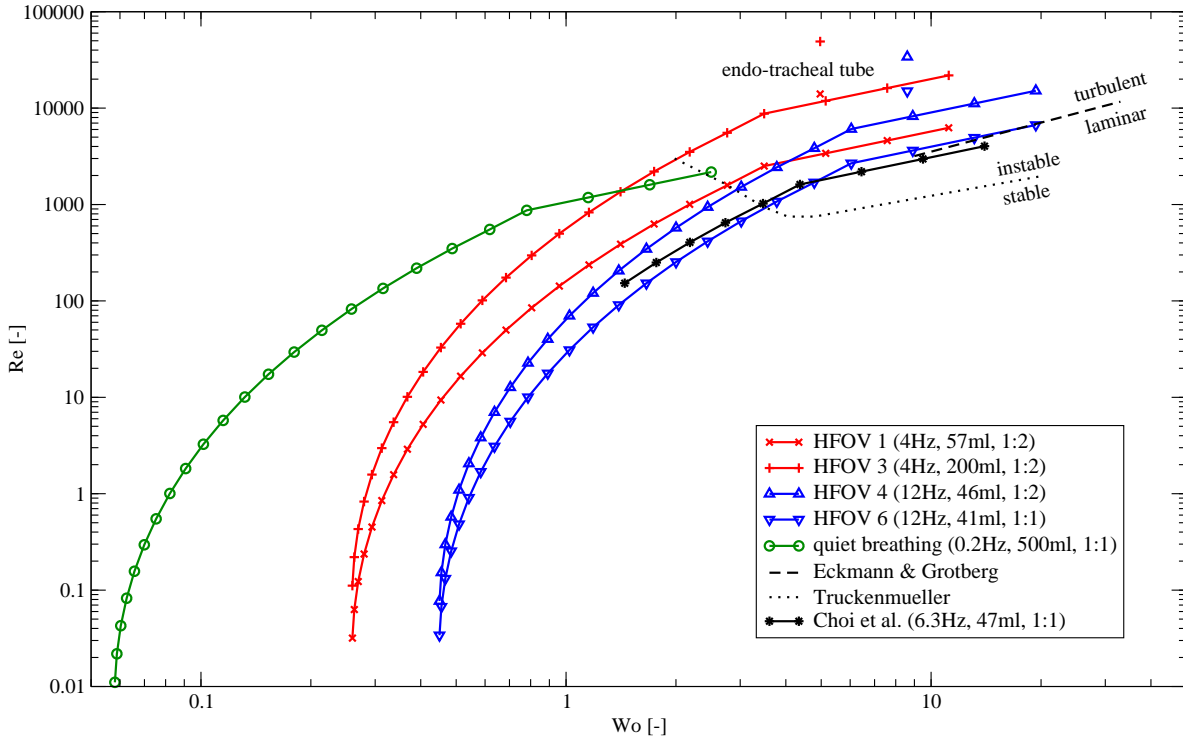


Figure 3. Parameter range in the bronchial tree under several respiratory conditions and at every single generation (symbols) including ETT. The frequency, the tidal volume and the in-/expiration ratio of each scenario are given in parentheses.

co-axial counter flow and is related to a phase shift of the near wall flow with respect to the core flow. In total the mean velocity develops a phase lag with respect to the driving pressure, which approaches $\pi/2$ for $Wo \rightarrow \infty$.

RESPIRATORY PARAMETERS

The human respiratory system forms a complex geometry with the central airways branching out in about 23 generations comprising over 1.6×10^7 single bronchi. According to Weibel (1963) the characteristic length scales range from roughly 18mm at the trachea down to $420\mu\text{m}$ at the alveolar level. Since in HFOV, typical tidal volumes V_{tidal} and frequencies also cover a broad range of ventilator settings, it is even more important to know the governing non-dimensional parameters of the expected flow regimes.

The most commonly used HFOV devices are pressure-cycle machines that neither monitor nor directly control the tidal volume and the flow rate $\partial_t V$, respectively. Moreover, the influence of the conducting parts of the ventilator device, the connector and the endo-tracheal tube (ETT) are more or less unknown and so are the actual flow rates delivered to the lung opening during HFOV. Hager *et al.* (2007) performed velocity measurements using a hot-wire anemometer attached between the y-connector of the HFOV device and the ETT in a test lung and ARDS patients to characterise the effects of ventilator settings (f , C , in-/expiratory ratio ($I:E$) et cetera) on the delivered tidal volumes. From his V_{tidal} data for four different scenarios we calculated the maximum flow rate at peak inspiration via $\partial_t V|_{max} = \pi \cdot f \cdot V_{tidal}$ under the assumption, that V_{tidal} is sinusoidally delivered to the lung opening

in $\Delta t = T/3$ for $I:E = 0.5$ and in $\Delta t = T/2$ for $I:E = 1$, respectively. Herewith, we estimate the parameter plane, shown in figure 3, for the whole bronchial tree and four relevant respirator settings compared to an average spontaneous breathing condition at peak inspiration. Each graph represents one scenario and each symbol of a graph represents the maximum Re and Wo in a bronchial tube at one specific generation. The right most symbols denote the trachea (generation 0), the left most symbols denote the lowest terminal bronchioles (generation 23) and the single symbols denote the corresponding situation in the ETT. The peak flow rates in each branch result from the simple assumption, that the flow rates subdivide according to the continuity equation (1) and the total cross-sectional area at each generation for a branching system of rigid tubes, where the geometrical parameters were taken from the classical airway model of Weibel (1963). To rate the parameter range in terms of transition to turbulence, figure 3 additionally shows experimental results from Eckmann & Grotberg (1991) and findings from a linear stability analysis of Trukenmüller (2006) for pure oscillatory pipe flow. Furthermore, the parameter regime of the numerical investigations performed by Choi *et al.* (2010) are given.

NUMERICAL METHODS

To solve the governing equations (1) and (2) in discretised form, we make use of an unstructured finite volume method based on the open source software package OpenFOAM. For temporal integration an implicit second-order backward differencing scheme is used, while the spatial discretisation is handled by an unbounded second-order central

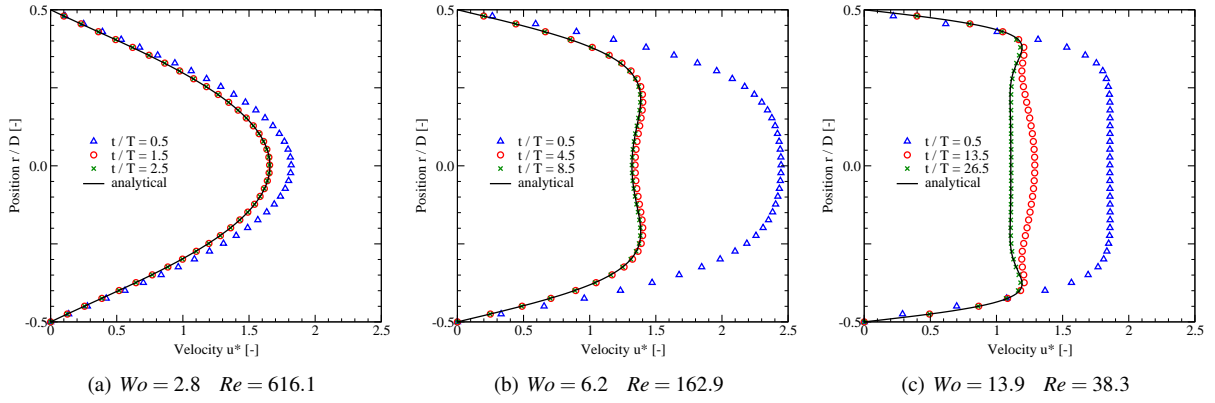


Figure 4. Normalised velocities obtained by numerical simulations (coloured symbols) in a generic bronchus for several Wo from breathing to HFOV after three different numbers of oscillation cycles compared to the analytical solution (black solid line).

differencing scheme. The solver takes advantage of the PISO method (pressure implicit with splitting of operators) for the pressure–velocity coupling and the resulting linear systems for the momentum equation and the Poisson equation are processed with a preconditioned bi–conjugate gradient solver and a generalised geometric–algebraic multi–grid solver, respectively.

We already mentioned in the introduction, that the flow field in the conducting airways is rather complex and, therefore, the velocity profiles at the boundaries are a priori unknown. Thus, we use pure Dirichlet BCs for the pressure and do not predefine a certain velocity profile at the open boundaries, which are in the case of HFOV all of these, inflow, outflow as well as mixed boundaries. In case of a single generic bronchus this leads to $p|_0 = C \cdot \sin(\omega \cdot t)$ and $p|_L = 0$, respectively. For the velocity we apply a mixed Dirichlet–Neumann BC at all open boundaries using a case–by–case analysis of the inward facing momentum flux Φ across each cell face. A Neumann condition, i.e. $\partial_x u|_{0,L} = 0$, is used for the outflow faces ($\Phi < 0$), whereas a velocity value is obtained from the face normal component of the internal cell value using $u|_{0,L} = \vec{u} \cdot \vec{n}$ for inflow faces ($\Phi \geq 0$). As a simplification at $r = D/2$ the standard no–slip and impermeability conditions are applied, despite the fact, that the bronchial walls are covered with cilia, mucus et cetera, which might have a relevant impact on the flow structure in terms of separation, transition and re–laminarisation. For all simulations, the time step is chosen to follow a Courant number of at least $Co \leq 0.3$ throughout the whole oscillation cycle.

NUMERICAL RESULTS

In order to validate the applied numerical method and the implementation of the time varying Dirichlet pressure BC, we simulated harmonic oscillatory flows. In this section we present the results for generic bronchi, an ETT, a symmetric bifurcation and a three–generation lung geometry.

OSCILLATORY PIPE FLOW

Here, we rate the numerical results using the analytical solution (6) for several Womersley parameters. According to figure 3, $Wo = 13.9$, $Wo = 6.2$ and $Wo = 2.8$ fall in the typ-

ical range of HFOV at the upper pulmonary airways, here the first seven generations. Moreover, the latter also represents the situation in quiet breathing at the trachea.

The computed laminar flow fields are in excellent agreement with the Womersley solution, as presented in figure 4. Non–dimensional radial velocity profiles are plotted after three different numbers of simulated oscillation cycles for $\omega \cdot t = \pi$, when the driving force becomes zero and changes its direction. Note, that the velocities are unequal zero at this phase, due to Wo well over unity and the resulting phase shift, as discussed earlier. Since the simulation starts from an initially resting fluid, the rising pressure gradient accelerates the air and causes an overshoot of the peak velocity. From figures 4(a) to 4(c) we conclude, that for increasing frequencies, i.e. higher Wo , a significantly longer settling phase (t/T) is required to let the flow field relax from the initial overshoot and converge to the analytical solution, due to a shorter deceleration phase. However, utilising the deviation of the numerical from the analytical results, defined as

$$\varepsilon(t) = \sum_{i=1}^{N_r} |u_{num}^*(r_i, t) - u_{ana}^*(r_i, t)| \Delta r_i \quad (7)$$

$$u^*(r, t) = \frac{u(r, t)}{\hat{u}_{ana}}, \quad (8)$$

we finally obtain an accuracy of at least $\varepsilon = 10^{-2}$ for all Wo on a structured hexahedral mesh with $N_r = 40$ equidistant grid points per radius. Nevertheless, HFOV simulations involving higher Wo take about 10 times more oscillation cycles to reach equilibrium when compared to spontaneous breathing simulations. We further found that applying an initial bulk velocity \vec{u} corresponding to the analytical solution at $t = 0$, reduces the settling phase by a factor of two. Initialising the exact Womersley profile would of course completely avoid this problem in the case of a straight pipe but does not work for irregular and multi–bifurcating airway geometries. Even though, the pressure amplitude (5) is identical for all three simulation, i.e. $\Delta p/L = 1.25 \text{ Pa/m}$, a higher frequency leads to a several times lower peak velocity \hat{u} . This is quantified by the decreasing Re shown in figure 4(a) to 4(c) and can be explained by means of equation (6). The rightmost term

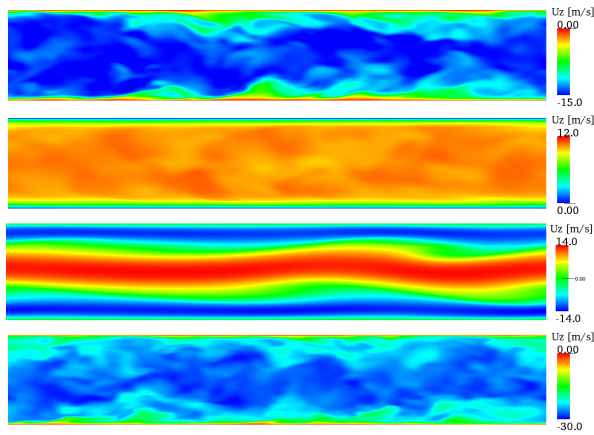


Figure 5. Instantaneous axial velocity fields for the case of HFOV 1 in the medial cross-section of the ETT at late expiration, early inspiration, flow reversal and early expiration (from top to bottom). Note the different scaling.

is more or less a periodic function of the Wo being responsible for the profile's shape, whereas the leftmost factor scales the profile according to the pressure amplitude C and the frequency ω . As stated earlier, this leads to much more deformed velocity profiles for increasing Wo . Therefore, HFVO simulations require finer grids to adequately resolve the stronger gradients ($\partial_r u$) occurring in the vicinity of the wall despite of relatively low Reynolds numbers. Furthermore, a higher pressure gradient is required to trigger a certain Re for a given Wo . In other words, an increasing ventilation frequency results in a significantly smaller flow rate through a certain bronchus for a given pressure gradient, which is also known from clinical practise (Hager *et al.* (2007)).

HFOV in the upper generations occasionally implies relatively high Re , at least when the peak flow rates occur. In this context, findings from Eckmann & Grotberg (1991) and Trukenmüller (2006) indicate, that the respiratory flow might not sustain laminar behaviour throughout the complete cycle, as shown in figure 3. Therefore, we also perform an implicit LES of an oscillating flow according to HFOV 1 in the ETT, using the same solver described before. However, here we use periodic BCs for the pressure and the velocity in axial direction, as well as an oscillating source term as driving force. The grid resolution was chosen to fulfil at least $\Delta x^+ = 14$, $r^+ \cdot \Delta\phi = \Delta r^+|_0 \leq 4.5$ as well as $\Delta r^+|_{D/2} = 0.82$ resulting in about 6.5×10^6 cells. Here, $+$ denotes wall units and the friction velocity u_τ within one cycle was a priori estimated by finding the maximum wall-normal velocity gradient of the analytical solution (6) for laminar flows. Using $Re = 1.8 \times 10^4$ and $Wo = 5$ from figure 3 we get $Re_\tau = 462$ and figure 5 presents instantaneous flow fields comprising turbulent expiration, re-laminarisation and large-scale instabilities during the flow reversal as well as re-establishing turbulence. Note, that the shown results are for the first simulated oscillation cycle on the mentioned grid, while the relaxation phase on coarser grid has taken less than 10 cycles.

OSCILLATORY BIFURCATION FLOW

We have also successfully used the pure Dirichlet pressure BC set-up to a three-dimensional symmetric bifurcation, employing the oscillatory pressure at the open end of the single parent tube. To demonstrate stable runs of oscillatory simulations comprising more than one additional open BC, we use identical as well as slightly different but constant pressure values at the distal ends of the two daughter tubes. The latter case is also a first approach to take uneven physiological behaviour of two different lung regions adjacent to the lower bifurcation ends into account. The unstructured mesh consists of about 5.5×10^5 tetrahedral and hexahedral cells, while the geometry consists of a 55° bifurcation and three tubes of 10 diameters in length. Figure 6 shows the flow fields obtained from the numerical simulations for $Wo = 13.9$ and for three different pressure set-ups with the exact values given in the caption. Since the velocity is plotted for $\omega \cdot t = 13/20 \cdot \pi$, which is for early inspiration, we can observe the co-axial counter flow phenomena in figure 6(a), as expected from the analytical Womersley solution for a straight pipe. Here, the inspiratory flow near the wall is indicated by the blue and the expiratory flow in the core regions is indicated by red colour, using

$$|\vec{u}| \cdot \frac{\vec{u} \cdot \vec{n}}{|\vec{u} \cdot \vec{n}|}, \quad (9)$$

where \vec{n} is the local cross-sectional normal vector. The flow field is completely symmetric for identical outlet pressure values and becomes more asymmetric with increasing pressure differences, as reflected in figures 6(b) and 6(c). In this case some of the fluid flows from the left daughter branch into the right one, getting more distinct for higher pressure differences. Similar flow structures can also occur in healthy and, more so, in diseased lungs due to uneven physiological behaviour of different airway regions in terms of variation in regional airway resistance or compliance.

OSCILLATORY FLOW IN A LUNG GEOMETRY

Finally, we performed first simulations of the flow in a three-generation lung geometry with multiple outlets reconstructed from computer tomography (CT) image data. The oscillating pressure BC was applied to the open trachea while the additional nine bronchial outlets maintain an identical pressure. The unstructured computational mesh consists of approximately 1.4×10^6 tetrahedral cells. Again, we use a typical HFOV frequency, resulting in $Wo = 13.9$ at the trachea, whereas the Reynolds number of $Re = 24.5$ is still not realistic. Figure 7 shows the lung geometry, the pressure distribution and the flow field in the trachea and at two bronchial outlets for $\omega \cdot t = 3/4\pi$, when the inlet pressure reaches its minimum and late expiration takes place. As mentioned earlier, here, a phase shift does also occur between the driving pressure and the bulk velocity due to a Womersley number well over one. Thus, we observe expiratory flow regions (red) close to the airway walls and an inspiratory core flow (blue) at the same time, using equation (9). This counter flow continuously exists throughout the whole geometry from the trachea down to lowest bronchi.

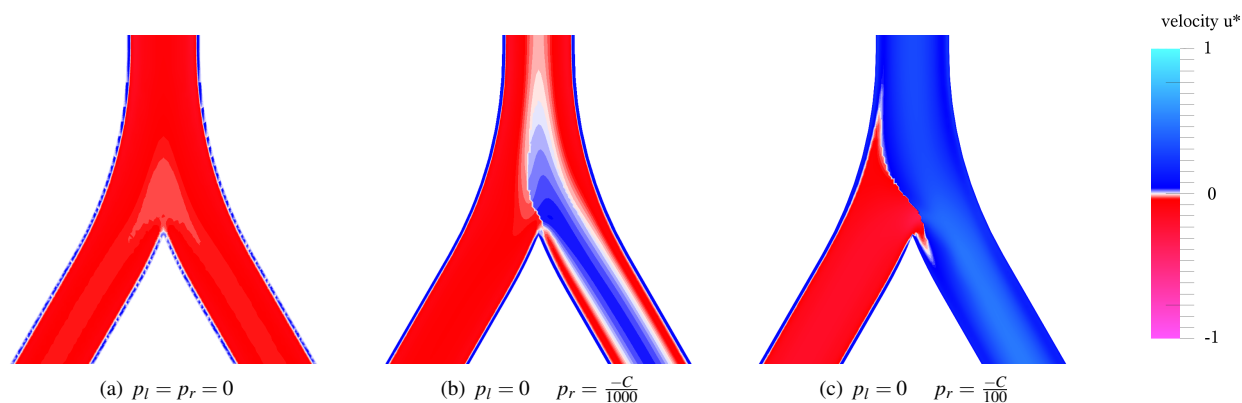


Figure 6. Close-up view of the normalised (8) velocity field in the coronal plane of the bifurcation at $\omega \cdot t = 13/20 \cdot \pi$ for $Wo = 13.9$ and for three different pressure set-ups at the lower left (p_l) and right (p_r) end, respectively.

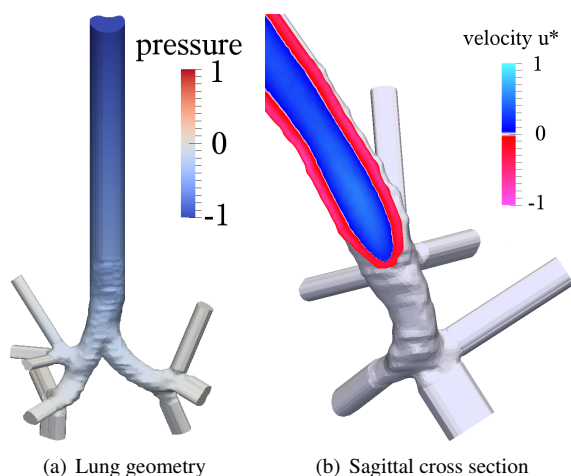


Figure 7. Pressure distribution in the entire lung model as well as velocity fields (9) in a sagittal cross section of the trachea at $\omega \cdot t = 3/4 \cdot \pi$ and for $Wo = 13.9$.

CONCLUSION

HFOV is an established artificial respiration technique in neonatology, providing potential benefits for the treatment of ARDS in adult patients. However, the advantages have not yet been translated into improved outcomes when compared to conventional ventilation, due to a lack of insight into the gas transport mechanisms. To improve this we perform numerical simulations of the oscillatory flow in simplified airway geometries using time varying Dirichlet BCs for the pressure and a second order accurate finite volume method. In the present contribution we presented numerical results of the oscillatory flow similar to that under conditions of HFOV in a straight pipe, a symmetric bifurcation and a three-generation airway geometry reconstructed from CT image data. It was demonstrated, that the use of Dirichlet pressure BCs allows to adequately reproduce the expected flow fields. For future simulations this allows the use of more realistic pressure BCs, such as non-harmonic pressure waves at the upper boundary, representing the HFOV device, and flow rate dependent pressure BCs at the distal ends at the same time.

Acknowledgment The authors would like to thank the *Deutsche Forschungsgesellschaft (DFG)* for providing financial support under grant WA 1510/8.

References

- Adler, K. & Brücker, C. 2007 Dynamic flow in a realistic model of the upper human lung airways. *Experiments in Fluids* **2–3**, 411–423.
- Choi, J., Xia, G., Tawhai, M., Hoffman, E. & Lin, C.-L. 2010 Numerical study of high-frequency oscillatory air flow and convective mixing in a CT-based human airway model. *Annals of Biomedical Engineering* **38**, 3550–3571.
- Eckmann, D. M. & Grotberg, J. B. 1991 Experiments on transition to turbulence in oscillatory pipe flow. *Journal of Fluid Mechanics* **222**, 329–350.
- Hager, D. N., Fessler, H. M., Kaczka, D. W., Shanholtz, C. B., Fuld, M. K., Simon, B. A. & Brower, R. G. 2007 Tidal volume delivery during high-frequency oscillatory ventilation in adults with acute respiratory distress syndrome. *Critical Care Medicine* **35**, 1522–1529.
- Krishnan, J. A. & Brower, R. G. 2000 High-frequency ventilation for acute lung injury and ARDS. *CHEST* **118** (3), 795–807.
- Scholz, A.-W. K., Krenkel, L., Terekhov, M., Friedrich, J., Rivoire, J., Köbrich, R., Wolf, U., Kalthoff, D., David, M., Wagner, C. & Schreiber, L. M. 2010 *Magnetic resonance imaging and computational fluid dynamics of high frequency oscillatory ventilation*. Springer.
- Trukenmüller, K. E. 2006 *Stabilitätstheorie für die oszillierende Rohrströmung*. PhD thesis, Helmut-Schmidt-Universität, Hamburg.
- Wall, W. A., Wiechert, L., Comerford, A. & Rausch, S. 2010 Towards a comprehensive computational model for the respiratory system. *International Journal for Numerical Methods in Biomedical Engineering* **26**, 807–827.
- Weibel, E. R. 1963 *Morphometry of the human lung*. New York: Academic Press.
- Womersley, J. R. 1955 Method for the calculation of velocity, rate of flow and viscous drag in arteries when the pressure gradient is known. *Journal of Physiology* **127**, 553–563.